Marine Pollution Bulletin xxx (xxxx) xxx–xxx

Contents lists available at ScienceDirect

Marine Pollution Bulletin

journal homepage: www.elsevier.com/locate/marpolbul

Rare earth elements mobility processes in an AMD-affected estuary: Huelva Estuary (SW Spain)

K.L. Lecomte[a,*], A.M. Sarmiento[b,c], J. Borrego[b], J.M. Nieto[b,c]

[a] CICTERRA CONICET-Universidad Nacional de Córdoba, Argentina
[b] Dpto. Ciencias de la Tierra, Universidad de Huelva, 21071 Huelva, Spain
[c] Research Center of Natural Resources, Health and the Environment, University of Huelva, 21071 Huelva, Spain

ARTICLE INFO

Keywords:
Rare earth elements
Mixing process
Acid drainage
Estuary

ABSTRACT

Huelva Estuary is a transition zone where REE-rich acidic waters interact with saline-alkaline seawater. This mixing process influences the geochemical and mineralogical characteristics of particulate and dissolved fractions. The Tinto River has > 11,000 μg L^{-1} dissolved REE (pH = 1.66), whereas seawater only reaches $8.75 \cdot 10^{-2}$ μg L^{-1} dissolved REE (pH = 7.87). REE-normalized patterns in "pH < 6 solutions" are parallel and show similarities, diminishing their concentration as pH increases. Sequential extraction performed on the generated precipitates of mixed solutions indicates that most REE are associated to the residual phase. In a second order, REE are associated with soluble salts at pH 3 and 3.5 whereas in sediments generated at pH 4 and 5, they are distributed in salts (1° extraction), poorly crystallized Fe-bearing minerals (schwertmannite, 3° extraction) and well crystallized Fe-bearing minerals (goethite - hematite, 4° extraction). Finally, precipitated REE are highest at pH 6 newly formed minerals with a release to solution in higher pH.

1. Introduction

Acid mine drainage (AMD) is the main environmental problem stemming from mining activities (e.g., Nordstrom, 1982; Sarmiento et al., 2009, 2011; Nieto et al., 2013). AMD is characterized by low pH and a high concentration of dissolved "toxic" elements, such as As, Pb, Zn, Sn, Cu, Cd, Cr, Ni, Mg, and also high concentration of rare earth elements (REE, e.g., Gammons et al., 2005; Pérez-López et al., 2010; Delgado et al., 2012; Sharifi et al., 2013). Relatively scarce information has been acquired to date on REE-associated biological effects, from studies of bioaccumulation and of bioassays on animal, plant and models; a few case reports have focused on human health effects following occupational REE exposures, in the present lack of epidemiological studies of occupationally exposed groups (Rim et al., 2013; Pagano et al., 2015). REE have similarities in ionic radii and chemical activities, they show coherent geochemical behavior in natural systems due to their similar physico-chemical properties. While they are freed during weathering, they are rapidly adsorbed onto colloids, and thus constitute valuable tracers of the original rock (e.g., Elderfield et al., 1990; Sholkovitz, 1995). Precipitated sediments in AMD systems are mostly iron oxides, which are important adsorbents of heavy metals, REE and other harmful elements. Adsorption capacity arises from a large specific surface area and from the development of surface charge. The specific surface area of iron oxides typically ranges from 100 to 200 m^2 g^{-1} in mining environments (Bigham et al., 1990; Gagliano et al., 2004). Iron oxide surfaces are protonated, and thus are positively charged in acidic conditions, while being dehydroxylated and negatively charged in alkaline conditions. The pH at which the surface has an equal amount of positive and negative adsorption sites is called the point of zero charge (PZC) and is measured by potentiometric titration.

Primarily because of tidal influences, geochemical processes controlling REE in estuarine systems are complex. The Huelva Estuary is a partially enclosed body of water along the coast, where acid drainage from the Tinto River meets and mixes with salt water from the Atlantic Ocean. This transitional area is influenced by tides, but protected from ocean waves, winds and storms by land forms including barrier islands peninsulas. This is a transitional area, where REE-rich acid waters interact with alkaline waters from the ocean, giving rise to multiple processes that control dissolved and particulate geochemical and mineralogical characteristics.

There are many studies of this area with diverse objectives. Most studies are related to the importance of polluting load of the region, which is considered to be one of most polluted systems in the world (e.g., Braungardt et al., 2003; Carro et al., 2007; Sarmiento et al., 2009; López-González et al., 2012; Asta et al., 2015; Lecomte et al., 2016a; Rosado et al., 2016). The interest in the elements during water/

* Corresponding author.
E-mail address: karina.lecomte@unc.edu.ar (K.L. Lecomte).

http://dx.doi.org/10.1016/j.marpolbul.2017.06.030
Received 16 May 2017; Received in revised form 7 June 2017; Accepted 8 June 2017

sediment interaction gives rise to a new study. Following this research, Lecomte et al. (2013, 2014) and Sarmiento et al. (2015) have analyzed metal mobility in this scenario. As the estuary's sediments can display two different origins (i.e., those produced on site by means of flocculation and precipitation, and those deriving from dynamic processes, such as fluvial input and tide), the authors aimed to analyze geochemical features from the site where they are deposited and to mix Tinto River and seawater samples in laboratory. However, there are few studies related to REE mobility in sequential extraction (e.g. Ayora et al., 2015; Prudêncio et al., 2015). Thus, this paper aims to reconstruct the conditions and processes occurring in nature, to identify and quantify the REE mobility (e.g., precipitation, adsorption/desorption by ICP-OES) during the pH gradient developed in the Huelva Estuary.

This work analyzes REE phase's distribution in the newly formed sediments generated when Tinto River reaches the seawater. For this purpose, the newly formed sediments from the mixing of Tinto River and Atlantic seawaters endmembers were used. Sequential extraction was used to evaluate the adsorption of REE in different phases and also at variable pH values. This study also determines the REE fractionation pattern related to acid–saline mixing processes.

2. Material and methods

2.1. Study site

Huelva estuarine is composed by the Tinto and Odiel Rivers (Fig. 1). The system is renowned for mining activities, which have taken place there going back to as early at the Roman Empire. The Tinto River drainage system includes an area of 1670 km^2 and the river/estuary extends for 95 km to its mouth near Huelva. The headwaters of the river (~400 m a.s.l.) are located in an area of intense mining. Downstream, at the town of Niebla (40 m a.s.l.), river meandering begins with a modest flood plain. This estuarine system is affected by a semidiurnal mesotidal regime; with a mean tidal range of 2.69 m (Borrego et al., 2004). The Tinto River discharge contribution is characterized by strong irregularity throughout the years. Mean monthly discharge is 8.4 Hm^3, while it may exceed 55 Hm^3 in the rainiest months. On the other hand, during the dry season (northern hemisphere summer months), river contribution is limited. Water quality of this estuary is extremely poor, with low tide pH values typically at 2.0–2.5. Flood tides bring in water from the Atlantic and raise the pH to near neutral levels in the lower portion of the estuary (Morales et al., 2008).

In April 2013, two endmember samples were collected: one from the Tinto River headwaters (37°40′31″N and 6°33′37″W) and the second in the coast of Huelva, Gulf of Cadiz (37°7′58″N and 6°51′43″W). The seawater sample was taken in a contamination-free underway; whereas nutrient levels, $^{228}Ra/^{226}Ra$ activity ratios, and Ni concentrations in coastal water of the Gulf of Cadiz were not exceptional for coastal environments, and there is no AMD interference since the marine currents are towards the Mediterranean Sea (Van Geen et al., 1991). Water temperature, pH, and electrical conductivity of both endmember samples were measured in situ. Seawater alkalinity was measured in unfiltered water as $CaCO_3$, using a 0.1600 N H_2SO_4 solution until an end point of pH = 4.5 was reached.

2.2. Water mixing experiment

To calculate the relation of Tinto River and seawater needed to reach a chosen pH, an experiment was conducted with representative samples of both systems. A pH controlled test was carried out by mixing a known volume of river water with enough seawater, until reaching selected pH. Due to the substantial seawater volume needed to reach pH 7, the mixing solutions were done on the coast of Huelva. Tinto River and seawater ratios were normalized to 1 L of Tinto River and seawater volume needed was the following: 170 L to reach pH 3; 280 L for pH 3.5; 320 L for pH 4; 492 L for pH 5; 840 L for pH 6 and 2000 L for pH 7. The amount of seawater to overcome Fe and Al buffer barriers is evident.

Six mixed solutions were performed, named KL3, when the solution reached a pH of 3; KL3.5, KL4, KL5, KL6 and KL7 at pH of 3.5, 4, 5, 6 and 7, respectively. After mixing, the sediments precipitated were collected. The precipitated sediment was collected by vacuum-filtered the solutions with 0.1-μm pore-size cellulose filters (HA-type, Millipore

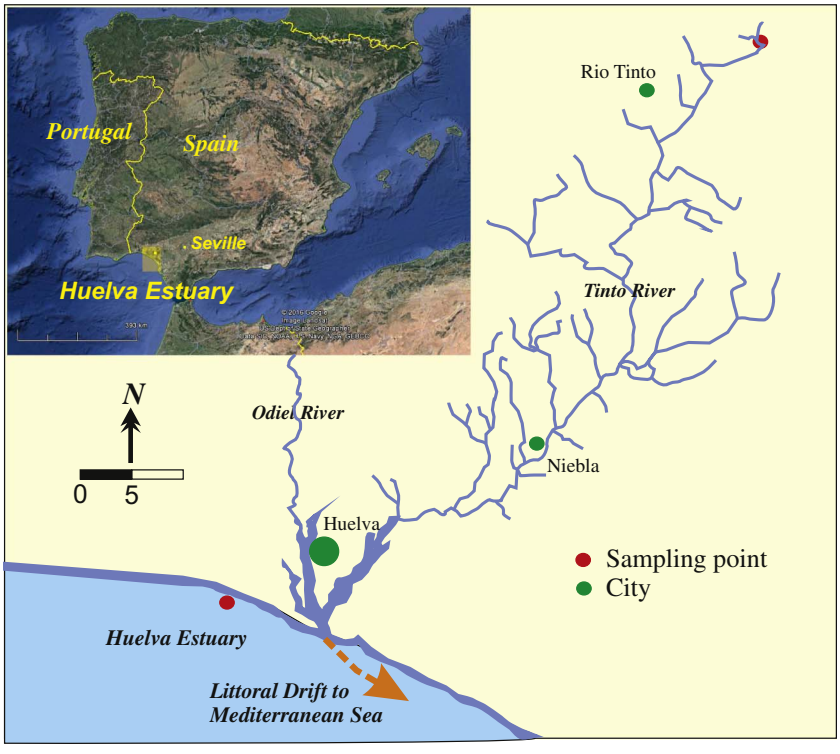

Fig. 1. Map showing Tinto River catchment, Huelva Estuary and study area.

Corp.). The sediment samples were prepared for the sequential extraction (SE) and the bulk extraction (BE) procedures.

2.3. Sequential extraction procedure

The sequential extraction procedure was done following Caraballo et al. (2009) methodology. Those authors adapted procedure from Dold (2003), where they made some modifications to the sample-extractant volume ratio and the time and nature of contact to adapt the method for samples with high concentrations of iron oxides and iron oxyhydroxysulfates (e.g., AMD systems). In this work, the fifth final step of Caraballo et al. (2009) methodology was also modified due to the absence of silicate in these new sediments.

Step 1) of the SE is the *water soluble fraction*. 200 mg of the sample were shaken with 20 mL deionizied water to dissolve secondary sulfates (e.g., gypsum) and other salts, which are very important in AMD environments. This step identifies the easily available contaminants (elements associated with sulfates and other salts). Due to their highly crystalline phases, a 12 h at room temperature (RT) shaking period was selected to ensure complete dissolution of all water-soluble minerals present in samples.

Step 2) refers to *sorbed and exchangeable fraction*. In this step, 20 mL 1 M NH_4-acetate solution was used for 1 h at RT to leach carbonates and some clay minerals and also to extract elements that are adsorbed to mineral surfaces (schwertmannite, goethite, and hydrobasaluminite). These metals are also characterized as available.

Step 3) implies *poorly ordered* Fe^{3+} *oxyhydroxides and oxyhydroxysulfates*. Schwertmannite, hydrobasaluminite and gibbsite were dissolved by 20 mL 0.2 M NH_4-oxalate, shaken for 30 min in darkness at RT. Fe, Al, SO_4^{2-} and co-precipitated elements were released.

Step 4) involves *highly ordered* Fe^{3+} *hydroxides and oxides*. The extractant used was again 20 mL 0.2 M NH_4-oxalate but in this case samples were exposed to light and heated to 80 °C in a water bath for 1 h to dissolved more crystalline iron precipitates (goethite).

In Step 5) *organic matter* was eliminated for 1 h by adding H_2O_2 35% at RT, and then heated at 85 °C in a water bath for 1 h. A 16 h room temperature (RT) shaking period was used with 25 mL 1 M NH_4-acetate extractant.

Finally, Step 6) is *residual digestion*. After the first five SE steps, the samples used in this step consist almost entirely of residual fraction of detrital and atmospheric particulate (quartz and clays). 5 mL aqua regia was used.

Accordingly, the digestion procedure developed for the total digestion of samples with organic and inorganic compounds was selected (Querol et al., 1996). Hydrofluoric acid was used to ensure the complete dissolution of inorganic materials, and $HClO_4$ and HNO_3 were used to dissolve the organic material.

In every step a blank was analyzed, according to the full treatment given to samples. Samples extracted from the SE were named XKL*n* or XBla, where X refers to the extraction step (from one to six), *n* identifies pH and Bla refers to blank samples.

2.4. Bulk extraction procedure

To validate the results, bulk extraction (BE) was also done to each of the original samples (named BKL*n*) following a procedure similar to Step 6 of the sequential extraction. The control of the results was performed following Quispe et al. (2012), by comparing the sum of the six steps of the sequential extraction with the results obtained from the BE, by calculating the recovery percentage:

$$\%\text{Recovery} = \frac{\text{Step 1} + \text{Step 2} + \text{Step 3} + \text{Step 4} + \text{Step 5} + \text{Step 6}}{\text{bulk extraction}} \times 100 \quad (1)$$

The mean recovery percentages of each sample were between 111% and 97% (mean 104 ± 6.1%) for each REE, except for Tb and Tm, which had recovery percentages of 80 ± 17% and 93 ± 17%, respectively. These favorable recovery values show the high reliability of the data obtained in this study. The relatively high standard deviation and low recovery values for some of Tb and Tm are a consequence of the very low concentrations analyzed for some samples, and therefore, the high variability should not affect the results considerably.

2.5. Analytical methodology

The aqueous chemistry of starting solutions and aliquots collected in the mixed samples was analyzed by inductively coupled plasma (Jobin ICP-MS Agilent 7700) in the LICAUH-CIDERTA laboratory of the University of Huelva. The chemical analysis was undertaken following a custom-designed protocol specific to AMD waters (Tyler et al., 2004). Certified Reference Materials (SARM 4 NORITE and SARM 1 GRANITE) were used to validate analytical measured methods and for the calibration of instrument. The results have been related by De la Rosa et al., 2001. Internal standards were used to correct for instrumental drift and matrix suppression for each sample. Repetitions were also used to check the accuracy and possible instrument signal drifting after every 10 samples. The detection limit for REE was always lower than 0.001 μg L^{-1}.

3. Results and discussion

3.1. Dissolved phases: initial samples and mixed solutions

In order to analyze REE referred to a patron, PAAS normalization was used, as identified with a subscript $_{SN}$. Table 1 shows REE dissolved concentrations, ΣREE, La_{SN}/Lu_{SN} ratios and Eu and Ce anomalies for the dissolved phases. Initial solutions are Tinto River (KLT) and seawater (KLM) endmembers samples, whereas mixed solutions are those generated by mixing KLT and KLM to generate the new solutions with determined pH values (i.e., 3, 3.5, 4, 5, 6, and 7).

REE dissolved concentrations in the natural environment are much lower than 1 μg L^{-1} (e.g., García et al., 2007; Gaillardet et al., 2014; Lecomte et al., 2016b). Particularly, Noack et al. (2014) present a comprehensive study of distribution of REE in ocean, groundwater, rivers and lakes, indicating REE concentration with medians < 1 μg L^{-1}. On the other hand, a strong correlation between high concentration of REE and acidity has been reported both in surface and ground waters, as well as in leaching studies of soils with different pH solutions (Fernandez-Caliani et al., 2009; Welch et al., 2009; Noack et al., 2014). However, in acid drainage systems, this concentration is increased by several orders of magnitude, due to low pH and the consequential desorption process (e.g., Gimeno Serrano et al., 2000; Protano and Riccobono, 2002; Borrego et al., 2005; Merten et al., 2005; Olías et al., 2005; Zhao et al., 2007; Da Silva et al., 2009; Welch et al., 2009; Borrego et al., 2012; Sahoo et al., 2012; Medas et al., 2013; Ayora et al., 2015, Migaszewski et al., 2016). Thus, the ΣREE concentrations in AMD published by these authors range from 50 and 126 μg L^{-1}. The Tinto River sample has extremely high REE values—one of the highest registered in natural environment—that range from 8 for Lu to 4480 μg L^{-1} for Ce, with ΣREE = 11,169 μg L^{-1}, representing a high outlier. On the other hand, seawater is a REE-diluted solution, with ΣREE = 0.092 μg L^{-1}.

Mixed solution samples present a range of ΣREE from the lowest to the highest pH. REE-concentrations decrease from ~80 μg L^{-1} in the sample at pH 3, to ~0.15 μg L^{-1} in the circumneutral sample. As is exhibited in Fig. 2, mixed samples show a high (r = 0.98) inverse relationship between REE dissolved concentration and pH. This means that dissolved REE concentrations decrease significantly in a gradient throughout the Estuary, from extreme values related to the river, to normal values found in waters diluted by the seawater. This behavior follows a polinomic equation as: ΣREE = 4.4 pH^2–63 pH + 222.

REE behavior is explained because of their concentration is

Table 1
REE concentration, ΣREE, La_{SN}/Lu_{SN} and anomalies of initial and mixed solutions. "bdl": below detection limit (< 0.001 μg L^{-1}).

Sample		KLT	KLM	KL3	KL3.5	KL4	KL5	KL6	KL7
pH		1.66	7.87	3.00	3.50	4.00	5.00	6.00	7.00
		Tinto River	Sea water	Mixed solutions					
La	μg L^{-1}	1.78E + 03	1.35E − 02	1.35E + 01	8.17E + 00	6.98E + 00	4.67E + 00	5.05E − 01	4.49E − 02
Ce		4.48E + 03	1.68E − 02	3.11E + 01	1.84E + 01	1.54E + 01	9.94E + 00	5.13E − 01	3.97E − 02
Pr		5.90E + 02	5.44E − 03	4.32E + 00	2.56E + 00	2.07E + 00	1.27E + 00	5.46E − 02	5.39E − 03
Nd		2.58E + 03	8.37E − 03	1.86E + 01	1.07E + 01	8.70E + 00	5.19E + 00	1.87E − 01	2.47E − 02
Sm		6.14E + 02	3.81E − 03	4.48E + 00	2.52E + 00	2.06E + 00	1.23E + 00	3.86E − 02	7.45E − 03
Eu		6.54E + 01	3.94E − 03	5.48E − 01	3.18E − 01	2.65E − 01	1.46E − 01	5.93E − 03	2.06E − 03
Gd		5.54E + 02	9.14E − 03	3.71E + 00	2.14E + 00	1.84E + 00	1.05E + 00	2.91E − 02	1.96E − 03
Tb		5.47E + 01	4.00E − 03	bdl	bdl	bdl	bdl	bdl	bdl
Dy		2.53E + 02	5.64E − 03	2.04E + 00	1.18E + 00	9.71E − 01	6.13E − 01	1.19E − 02	3.66E − 03
Ho		3.72E + 01	3.50E − 03	3.18E − 01	1.84E − 01	1.48E − 01	9.51E − 02	1.58E − 03	5.04E − 04
Er		8.59E + 01	7.08E − 03	7.10E − 01	4.24E − 01	3.41E − 01	2.09E − 01	6.18E − 03	4.89E − 03
Tm		1.02E + 01	3.62E − 03	8.58E − 02	5.32E − 02	3.74E − 02	2.52E − 02	1.98E − 03	3.52E − 04
Yb		6.17E + 01	3.71E − 03	5.25E − 01	3.17E − 01	2.39E − 01	1.40E − 01	6.94E − 03	5.25E − 03
Lu		7.63E + 00	2.97E − 03	7.47E − 02	3.78E − 02	3.53E − 02	1.85E − 02	1.30E − 03	1.71E − 03
ΣREE		1.12E + 04	9.15E − 02	8.00E + 01	4.70E + 01	3.91E + 01	2.46E + 01	1.36E + 00	1.42E − 01
La_{SN}/Lu_{SN}		2.64	0.05	2.05	2.45	2.24	2.86	4.40	0.30
Eu*		0.53	2.76	0.63	0.64	0.64	0.60	0.83	2.17
Ce*		0.99	0.44	0.93	0.92	0.93	0.94	0.66	0.56

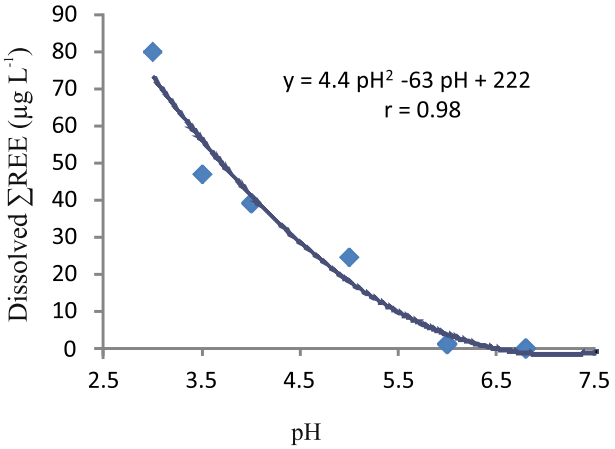

Fig. 2. Scatter diagram showing the relation between dissolved REE and pH variation.

extremely high in the river while practically null in the seawater. As was exposed, lower pH samples correspond to those mixing with less amount of seawater endmember. In this way, the amount of REE in each mixture is governed by the amount of both endmembers needed. As the pH of the mixed solution is increased, the amount of seawater required increases noticeably. This generates a sort of dilution accompanied by the precipitation of the new minerals, which increasingly include REE. The process generates sediments with a maximum of REE at pH 6, while it is inverted in the less acidic solution, releasing part of the adsorbed REE to the solution.

REE concentrations were normalized to past Post Archean Australian shale (PAAS) to identify their pattern and to compare them with other environments. Fig. 3 analyzes initial and mixed solutions. Tinto River sample (KLT) highest concentrations reached as much as two orders of magnitude. The figure shows that PAAS-normalized patterns are similar within the lower pH solutions (Tinto River and solution with pH < 6), with a relative enrichment of the middle-REE (MREE, Sm to Dy) over light-REE (LREE, La to Nd) and heavy-REE (HREE, Ho to Lu). Most REE normalized diagrams from granite-dominated, volcanic sedimentary environments and estuaries sediments show this REE pattern (e.g., Hannigan and Sholkovitz, 2001, Pasquini et al., 2004, Lecomte, 2006, García et al., 2007, Lecomte et al., 2008, and references therein). This pattern is also evident in AMD (e.g., Protano and Riccobono, 2002; Olías et al., 2005; Pérez-López et al., 2010; Ayora et al., 2015; Prudêncio et al., 2015). The figure also shows the predominance of LREE over HREE, with relatively constant La_{SN}/Lu_{SN} ratios, higher than 2 (mean 2.45, Table 1). This indicates that in acidic waters, LREE are preferentially in the dissolved phases. These "pH < 6 samples" also show negative Eu anomalies (Eu*) and almost no Ce anomalies (Ce*). They range from 0.53 to 0.64, and 0.92 to 0.99, respectively (Table 1). However, when circumneutral samples are analyzed (i.e., KL7 and seawater, pH > 6), REE concentrations are near detection limit and the interpretation made here only represents a qualitative tendency. In addition to their lowest concentrations, they display a predominance of HREE over MREE and LREE. Gaillardet et al. (1997) indicate that high pH river waters have the most enriched HREE patterns, close to that of seawater. This is also shown by La_{SN}/Lu_{SN} ratios < 1 (0.30 and 0.05, respectively, Table 1), suggesting a tendency of LREE depletion when pH becomes alkaline. They also show positive Eu* (2.17 and 2.76) and negative Ce* (0.56 and 0.44), differentiating their patterns from acid solutions, in agreement with Ayora et al. (2015). Finally, sample KL6 seems to transition between the two groups.

Eu* is widely used in petrology, due to its positive (enrichment) or negative (depletion) value, which results from the substitution of Sr by Eu in both feldspars (notably in Ca-plagioclase) and in carbonates (McLennan, 1989). It can be seen a negative Eu anomaly typical of AMD-affected waters (Pérez-López et al., 2010) in samples with higher proportion of AMD and lower pH. This is a direct consequence of recently formed acidic minerals, i.e., when sediments precipitate in a pH < 6 solution, they preferentially adsorb Eu over other REE. On the other hand, when pH > 6, newly formed minerals adsorbed Eu in less magnitude than other REE. Likewise, negative Ce* becomes more negative as pH increases, due to the preferential fractionation of Ce in oxyhydroxides of Fe (Olías et al., 2005), and in response to the oxidation of Ce^{+3} to Ce^{+4} and its subsequent precipitation from solution as CeO_2 (Brookins, 1989). This is evident in the negative relationship between Ce* and pH, as shown in Fig. 3 *insert*. The Ce* signature of seawater is preserved in samples with higher proportion of seawater (e.g., representing a higher pH) (Leybourne et al., 2000; Nozaky et al., 2000).

3.2. Precipitated phases

In this section, the particulate fractions scavenged from sediments

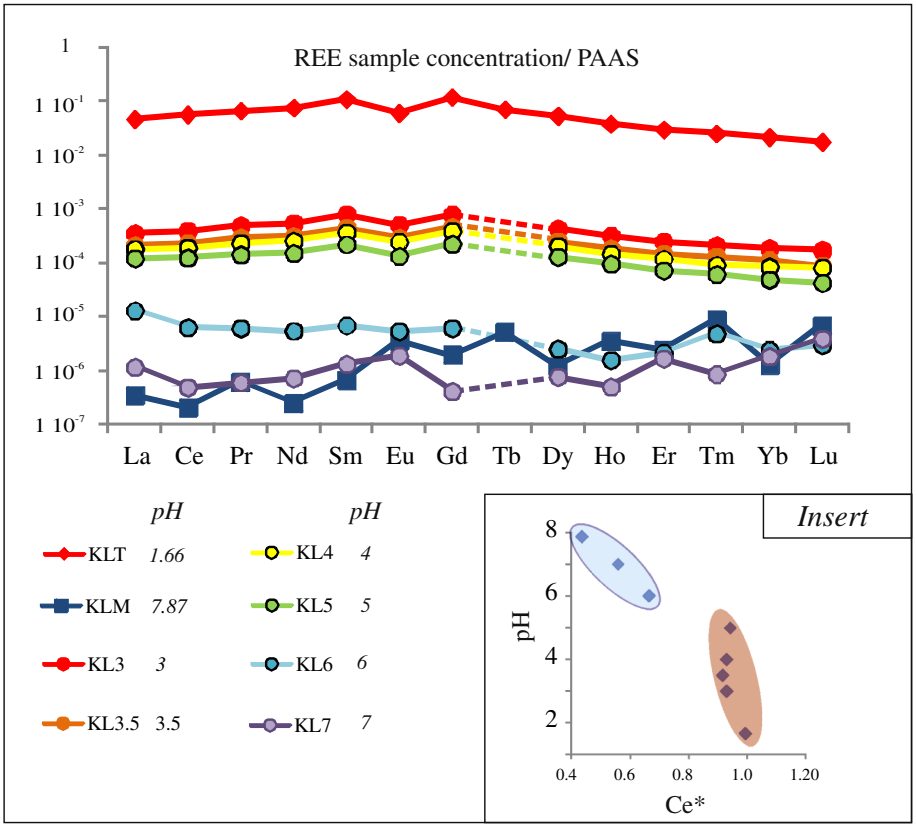

Fig. 3. The PAAS-normalized REE distribution patterns for Tinto River, seawater and mixed solutions at a pH gradient. Insert: Relation between Ce anomaly and pH, differentiating pH < 6 solutions from those near neutral pH.

have been analyzed. Sequential extraction was done in each newly sediment precipitated when mixing both initial solutions. It is known that REE are retained by sediments like Fe oxyhydroxides in AMD (e.g., Prudêncio et al., 2011, 2015 etc.), and it is also evident here.

The REE concentration of bulk extraction and each extracted phase are listed in Table 2, as well as anomalies and some chemical relationships. There is a high relation between bulk extraction and the sum of each extraction in sediments, for each REE. Moreover, the % recovery of each analyzed element presents differences are mostly < 10%. Results < 100% are exhibited principally in sediment generated at pH 7, which can be explained by those values "below detection limits."

Results presented in the present work, show differences compared with REE concentration in López-González et al. (2012) of the Huelva Estuary. In the present work—without any extra influence—present significantly lower concentrations than in López-González et al. (2012), where ΣREE range between 55.8 (pH 3) and 1502.1 (pH 6) μg kg^{-1}, and in mixed origin sediments, present ΣREE from 32,900 (pH 7.54) to 154,900 (pH 7.26) μg L^{-1}. This suggests that López-González et al. (2012) overestimated REE from adsorption processes. As an example, La in sample S5 (corresponding to sediment sampled at a pH 3.02) and in sample S1 (near the mouth of the river, with pH 7.74) shows a concentration range from 117,500 to 188,400 μg L^{-1}, whereas in this present work, La ranges from 9.67 to 220.2 μg L^{-1}. This seems that taking samples with mixed origins creates a homogenization of marked differences between variable pH samples.

Fig. 4a and b illustrates the ΣREE concentration from each extraction in each mixed solution (i.e., results in μg L^{-1} and in percentage, respectively). Generally, as predicted, REE increase their concentration in sediments generated at a higher pH, reaching a maximum at pH 6 (i.e., > 1700 μg L^{-1}, sky-blue line in Fig. 4a), whereas at around pH 7, REE concentration start to reduce again. This scheme is also evidenced by other elements, for example As, Cu, and Zn (Lecomte et al., 2014; Sarmiento et al., 2015). This could be explained if the PZC is near pH 6 for the adsorption/desorption process for oxy-hydroxides and oxyhydroxysulfates, which yield in REE released to solution.

The last extraction (Extraction 6) has the most concentrated REE, indicating the residual phase, i.e., forming mineral structure; ranging between < 60% to ~80%. The sediment generated at pH 3 shows the lowest REE concentration. In the same way, the lowest ΣREE sediment concentration corresponds to the lowest pH. It is noticeable that, excepting residual phase, sediments generated at these pH (i.e., 3, 3.5, 4) present REE concentrations distributed largely in soluble salts, which are represented by the 1° extraction. Extraction 3 and 4 correspond to "poorly and highly ordered Fe oxy-hydroxides," respectively, and they also have an important stake in the sediment generated at less acidic solution. Soluble salts represent ~20% in pH 3.5 and 4; whereas Fe oxy-hydroxides are characterized with 9 to > 15%. On the other hand, sediments from higher pH levels (i.e., 6 and 7) show their REE associated—in a range between 23 and 42%—to Fe oxy-hydroxides phases (Extractions 3 and 4). Within this two phases, > 60% REE are represented by poorly crystallized minerals, such as schwertmannite, whereas highly ordered Fe^{3+} hydroxides and oxides are present in smaller amounts. In these samples, soluble salts are irrelevant.

Extraction 2 is represented by sorbed and exchangeable fraction in carbonates and clay minerals. As this is an acidic environment, carbonates are negligible, so this extraction can be interpreted as elements associated with clay minerals. In Fig. 4 and Table 2, it is evident that the clay phase only contributed with ~0.4%. In Extraction 5 organic matter was eliminated, and elements associated with this phase are also insignificant.

The REE adsorbed at pH 5 show transitional characteristics, with mean concentrations of REE both in salts (~9%), and Fe oxy-hydroxides (20%). Here, fractions 2 and 5 (clay minerals and organic matter) are also insignificant.

3.2.1. PAAS normalized REE pattern

Sequential extraction results were also normalized to PAAS to

Table 2
REE concentration, ΣREE, La_{SN}/Lu_{SN}, La_{SN}/Gd_{SN} and anomalies of sequential extractions. "bdl": below detection limit (< 0.001 μg L^{-1}).

Sample			La	Ce	Pr	Nd	Sm	Eu	Gd	Tb	Dy	Ho	Er	Tm	Yb	Lu	ΣREE	La_N/Lu_N	La_N/Gd_N	Eu*	Ce*
	pH		μg L^{-1}																		
1KL3	*3*	1° extraction	9.07E − 01	2.85E + 00	4.07E − 01	1.87E + 00	4.66E − 01	6.95E − 02	3.76E − 01	bdl	2.22E − 01	3.14E − 02	1.07E − 01	1.38E − 02	7.12E − 02	7.18E − 03	7.40	1.43	0.29	0.78	1.02
1KL3.5	*3.5*	(soluble salts)	3.17E + 00	1.18E + 01	1.91E + 00	9.02E + 00	2.22E + 00	3.03E − 01	1.60E + 00	bdl	9.69E − 01	1.47E − 01	3.76E − 01	4.76E − 02	2.96E − 01	3.03E − 02	31.9	1.19	0.24	0.76	0.99
1KL4	*4*		5.89E + 00	2.28E + 01	3.77E + 00	1.76E + 01	4.64E + 00	5.80E − 01	3.16E + 00	1.16E − 01	1.95E + 00	2.96E − 01	7.38E − 01	9.63E − 02	6.17E − 01	7.85E − 02	62.3	0.85	0.23	0.71	0.99
1KL5	*5*		6.13E + 00	1.73E + 01	2.29E + 00	9.43E + 00	2.22E + 00	2.91E − 01	1.90E + 00	bdl	1.05E + 00	1.48E − 01	3.25E − 01	3.25E − 02	2.12E − 01	2.05E − 02	41.4	3.39	0.39	0.67	1.04
1KL6	*6*		6.29E − 02	5.08E − 02	bdl	1.85E − 03	bdl	9.60E − 04	1.23E − 03	bdl	bdl	bdl	bdl	bdl	bdl	bdl	0.12	–	6.24	6.74	0.78
1KL7	*7*		bdl	bdl	bdl	bdl	bdl	bdl	bdl	bdl	bdl	bdl	bdl	bdl	bdl	bdl	bdl	–	–	–	–
2KL3	*3*	2° extraction	1.22E − 02	2.26E − 02	6.94E − 03	2.91E − 02	1.79E − 02	4.83E − 03	1.44E − 02	bdl	1.09E − 02	3.77E − 03	3.33E − 03	2.31E − 03	3.68E − 03	3.88E − 03	0.14	0.04	0.10	1.41	0.51
2KL3.5	*3.5*	(carbonates - clays)	1.02E − 02	4.19E − 02	1.02E − 02	7.63E − 02	3.83E − 02	6.37E − 03	2.94E − 02	bdl	2.20E − 02	3.07E − 03	4.84E − 03	1.22E − 03	3.40E − 03	1.92E − 03	0.25	0.06	0.04	0.89	0.74
2KL4	*4*		2.75E − 02	1.07E − 01	2.01E − 02	1.05E − 01	7.27E − 02	1.34E − 02	5.43E − 02	bdl	3.53E − 02	7.73E − 03	1.25E − 02	5.35E − 03	1.18E − 02	5.46E − 03	0.48	0.06	0.06	1.00	0.90
2KL5	*5*		1.06E − 01	3.93E − 01	7.29E − 02	3.79E − 01	1.64E − 01	1.81E − 02	1.02E − 01	bdl	5.70E − 02	7.09E − 03	2.24E − 02	3.29E − 03	2.17E − 02	2.34E − 03	1.35	0.51	0.13	0.65	0.89
2KL6	*6*		1.40E + 00	2.37E + 00	3.18E − 01	1.44E + 00	3.45E − 01	5.13E − 02	3.18E − 01	bdl	1.31E − 01	1.87E − 02	3.51E − 02	3.17E − 03	1.51E − 02	2.66E − 03	6.45	5.97	0.54	0.73	0.82
2KL7	*7*		4.98E − 01	8.27E − 01	1.13E − 01	5.17E − 01	1.49E − 01	1.88E − 02	1.43E − 01	bdl	5.24E − 02	5.58E − 03	1.11E − 02	1.67E − 03	9.53E − 03	1.19E − 03	2.35	4.76	0.43	0.61	0.80
3KL3	*3*	3° extraction (Fe	3.04E − 01	8.62E − 01	1.29E − 01	6.06E − 01	1.70E − 01	3.69E − 02	1.56E − 01	bdl	1.13E − 01	2.07E − 02	5.50E − 02	7.06E − 03	5.15E − 02	7.66E − 03	2.52	0.45	0.24	1.07	0.96
3KL3.5	*3.5*	oxihidroxides poor	6.71E − 01	2.79E + 00	5.04E − 01	2.70E + 00	7.94E − 01	1.02E − 01	6.12E − 01	bdl	4.52E − 01	7.12E − 02	2.32E − 01	2.42E − 02	1.62E − 01	1.94E − 02	9.14	0.39	0.13	0.69	0.94
3KL4	*4*	cristalized)	1.38E + 00	5.79E + 00	1.08E + 00	5.74E + 00	1.77E + 00	2.58E − 01	1.41E + 00	bdl	9.75E − 01	1.51E − 01	4.37E − 01	6.03E − 02	3.92E − 01	4.89E − 02	19.5	0.32	0.12	0.77	0.92
3KL5	*5*		4.08E + 00	1.83E + 01	3.18E + 00	1.68E + 01	5.49E + 00	7.19E − 01	4.35E + 00	4.11E − 02	2.87E + 00	4.25E − 01	9.83E − 01	1.58E − 01	8.76E − 01	1.21E − 01	58.4	0.38	0.11	0.69	0.99
3KL6	*6*		4.06E + 01	9.49E + 01	1.31E + 01	5.46E + 01	1.38E + 01	2.08E + 00	1.49E + 01	1.42E + 00	9.53E + 00	1.46E + 00	3.32E + 00	4.00E − 01	2.17E + 00	3.41E − 01	253	1.35	0.33	0.68	0.94
3KL7	*7*		2.30E + 01	5.19E + 01	7.00E + 00	2.97E + 01	7.19E + 00	1.07E + 00	7.18E + 00	9.74E − 01	4.84E + 00	7.48E − 01	1.81E + 00	2.30E − 01	1.29E + 00	1.97E − 01	137	1.32	0.39	0.70	0.94
4KL3	*3*	4° extraction (highly	4.93E − 01	1.26E + 00	2.12E − 01	9.95E − 01	3.37E − 01	7.40E − 02	3.65E − 01	6.85E − 02	2.70E − 01	6.42E − 02	1.44E − 01	4.06E − 02	1.22E − 01	4.34E − 02	4.49	0.13	0.16	0.98	0.86
4KL3.5	*3.5*	ordered Fe^{3+}	8.09E − 01	3.06E + 00	5.58E − 01	3.08E + 00	1.07E + 00	1.56E − 01	1.01E + 00	1.56E − 01	7.95E − 01	1.42E − 01	3.57E − 01	5.25E − 02	3.29E − 01	4.19E − 02	11.6	0.22	0.10	0.70	0.91
4KL4	*4*	hydroxides and	1.69E + 00	7.13E + 00	1.35E + 00	7.62E + 00	2.75E + 00	4.02E − 01	2.46E + 00	3.75E − 01	2.12E + 00	3.60E − 01	9.43E − 01	1.36E − 01	8.30E − 01	9.96E − 02	28.3	0.19	0.08	0.73	0.91
4KL5	*5*	oxides)	2.37E + 00	1.00E + 01	1.78E + 00	9.03E + 00	3.07E + 00	4.53E − 01	2.54E + 00	3.81E − 01	1.94E + 00	3.23E − 01	8.04E − 01	1.21E − 01	7.25E − 01	1.10E − 01	33.7	0.24	0.11	0.76	0.95
4KL6	*6*		1.88E + 01	4.84E + 01	6.64E + 00	3.05E + 01	8.86E + 00	1.32E + 00	1.02E + 01	1.47E + 00	7.79E + 00	1.29E + 00	3.12E + 00	3.82E − 01	2.41E + 00	3.39E − 01	142	0.63	0.22	0.64	0.98
4KL7	*7*		1.20E + 01	2.97E + 01	4.05E + 00	1.77E + 01	4.87E + 00	6.96E − 01	5.24E + 00	7.18E − 01	3.69E + 00	5.97E − 01	1.52E + 00	1.75E − 01	1.16E + 00	1.42E − 01	82.3	0.96	0.28	0.64	0.96
5KL3	*3*	5° extraction	1.37E − 02	1.56E − 02	1.63E − 02	1.26E − 02	1.39E − 02	1.30E − 02	1.55E − 02	1.75E − 02	2.20E − 02	1.55E − 02	2.13E − 02	1.44E − 02	2.13E − 02	1.33E − 02	0.23	0.01	0.11	4.11	0.18
5KL3.5	*3.5*	(organic matter)	bdl	3.00E − 03	2.50E − 04	bdl	bdl	bdl	bdl	bdl	bdl	bdl	bdl	bdl	bdl	bdl	3.25E − 03	–	–	–	2.67
5KL4	*4*		1.72E − 03	1.61E − 02	1.62E − 03	3.23E − 02	bdl	bdl	bdl	bdl	bdl	bdl	bdl	bdl	bdl	bdl	0.05	–	–	–	1.77
5KL5	*5*		9.74E − 03	5.06E − 02	6.13E − 03	3.37E − 02	4.71E − 03	bdl	5.72E − 03	1.12E − 03	4.11E − 03	bdl	bdl	bdl	2.00E − 04	bdl	0.12	–	0.21	–	1.34
5KL6	*6*		3.34E − 01	6.82E − 01	9.00E − 02	4.26E − 01	1.07E − 01	8.09E − 03	1.18E − 01	1.09E − 02	4.49E − 02	2.31E − 03	1.03E − 02	bdl	3.41E − 03	bdl	1.84	–	0.35	0.34	0.90
5KL7	*7*		6.77E − 02	1.04E − 01	1.89E − 02	8.40E − 02	1.54E − 02	bdl	6.95E − 03	1.36E − 03	5.48E − 03	bdl	bdl	bdl	bdl	bdl	0.30	–	1.19	–	0.67
6KL3	*3*	6° extraction	1.26E + 01	2.62E + 01	3.41E + 00	1.34E + 01	2.58E + 00	4.15E − 01	1.62E + 00	1.78E − 01	8.19E − 01	1.20E − 01	3.19E − 01	3.51E − 02	2.61E − 01	3.54E − 02	62.0	4.05	0.95	0.94	0.92
6KL3.5	*3.5*	(residual fraction)	1.82E + 01	4.58E + 01	6.66E + 00	2.90E + 01	6.07E + 00	8.06E − 01	3.57E + 00	3.84E − 01	1.62E + 00	2.39E − 01	5.85E − 01	6.91E − 02	4.71E − 01	5.24E − 02	114	3.93	0.62	0.80	0.94
6KL4	*4*		2.66E + 01	7.95E + 01	1.27E + 01	5.81E + 01	1.29E + 01	1.53E + 00	7.22E + 00	7.48E − 01	3.15E + 00	4.53E − 01	1.14E + 00	1.52E − 01	9.56E − 01	1.04E − 01	205	2.89	0.45	0.73	0.93
6KL5	*5*		3.53E + 01	1.24E + 02	2.00E + 01	9.19E + 01	2.37E + 01	2.86E + 00	1.41E + 01	1.63E + 00	7.07E + 00	9.78E − 01	2.33E + 00	3.05E − 01	2.10E + 00	2.44E − 01	326	1.64	0.31	0.73	0.98
6KL6	*6*		1.99E + 02	5.47E + 02	7.09E + 01	3.05E + 02	7.03E + 01	8.99E + 00	5.80E + 01	6.70E + 00	3.00E + 01	4.47E + 00	1.03E + 01	1.26E + 00	7.58E + 00	9.33E − 01	1320	2.41	0.42	0.66	1.04
6KL7	*7*		5.06E + 01	1.26E + 02	1.64E + 01	7.00E + 01	1.52E + 01	1.97E + 00	1.16E + 01	1.30E + 00	5.57E + 00	8.16E − 01	1.92E + 00	2.24E − 01	1.35E + 00	1.72E − 01	303	3.34	0.53	0.70	0.99
BKL3	*3*	Pseudo- total	9.67E + 00	2.19E + 01	3.03E + 00	1.30E + 01	2.81E + 00	4.55E − 01	2.07E + 00	2.66E − 01	1.28E + 00	2.16E − 01	5.61E − 01	8.03E − 02	5.13E − 01	6.09E − 02	55.8	1.80	0.57	0.89	0.92
BKL3.5	*3.5*		1.81E + 01	5.31E + 01	8.41E + 00	3.96E + 01	9.43E + 00	1.29E + 00	6.31E + 00	7.92E − 01	3.84E + 00	6.26E − 01	1.57E + 00	2.13E − 01	1.32E + 00	1.65E − 01	145	1.24	0.35	0.78	0.94
BKL4	*4*		2.68E + 01	9.33E + 01	1.58E + 01	7.64E + 01	1.94E + 01	2.41E + 00	1.29E + 01	1.61E + 00	7.70E + 00	1.21E + 00	3.12E + 00	4.13E − 01	2.67E + 00	3.23E − 01	264	0.94	0.25	0.71	0.94
BKL5	*5*		4.54E + 01	1.71E + 02	2.84E + 01	1.32E + 02	3.58E + 01	4.64E + 00	2.42E + 01	3.04E + 00	1.40E + 01	2.08E + 00	4.95E + 00	6.48E − 01	4.42E + 00	5.10E − 01	472	1.01	0.23	0.74	0.98
BKL6	*6*		2.20E + 02	5.97E + 02	7.87E + 01	3.47E + 02	8.26E + 01	1.09E + 01	7.53E + 01	9.24E + 00	4.32E + 01	6.75E + 00	1.59E + 01	1.90E + 00	1.17E + 01	1.48E + 00	1502	1.69	0.36	0.65	1.02
BKL7	*7*		1.25E + 02	3.22E + 02	4.10E + 01	1.79E + 02	4.21E + 01	5.68E + 00	3.84E + 01	4.65E + 00	2.20E + 01	3.53E + 00	8.35E + 00	1.03E + 00	6.25E + 00	7.81E − 01	799	1.81	0.40	0.66	1.02

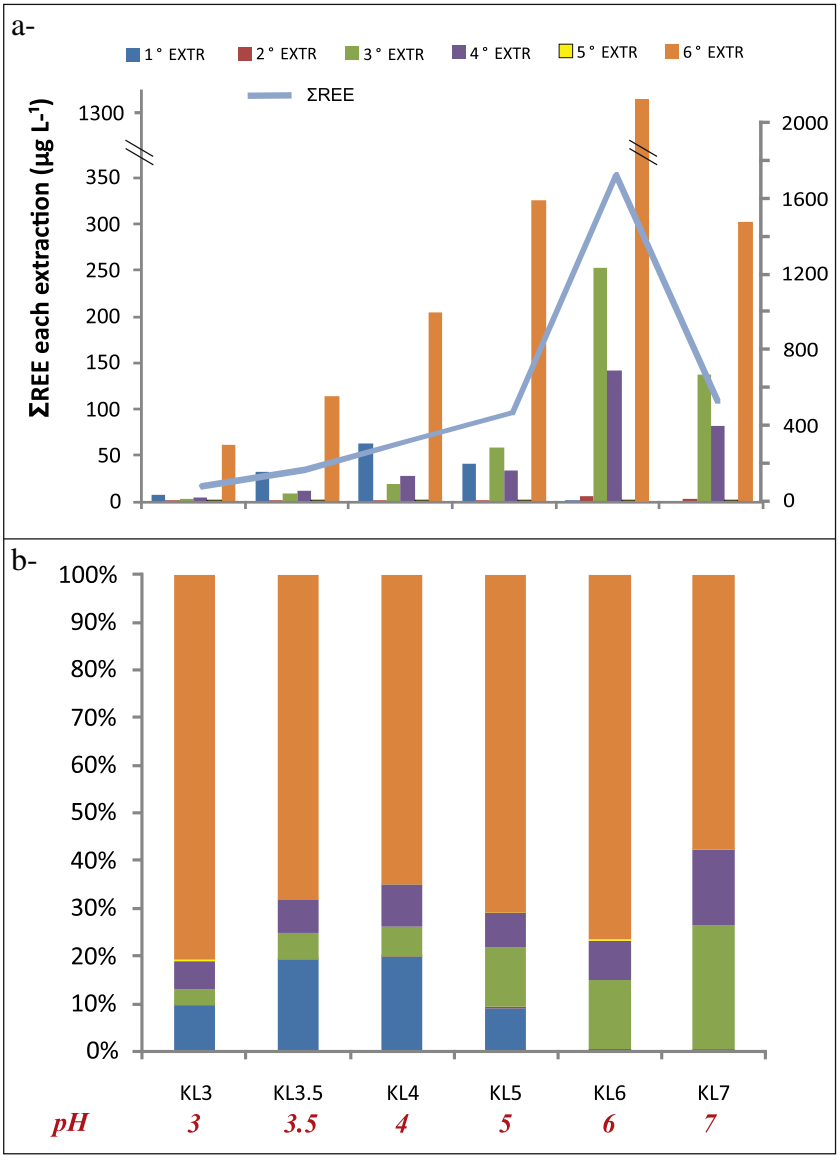

Fig. 4. REE concentration measured in each extracted phase for each pH solution, a)µg L^{-1}, and b) %.

analyze the behavior of each element. Fig. 5 shows the normalized diagrams of each extraction: Fig. 5a corresponds to extraction 1, and so on

Normalized values range between 2 and 7 orders of magnitude less than PAAS concentrations. As described before, the residual phase (Fig. 5f) is the most concentrated phase, followed by Fe oxy-hydroxides phases (Fig. 5c and d). Most patterns are similar; they present a preeminence of MREE over LREE and HREE. Generally, Samples 6 and 7 have the highest concentrations, except in soluble salts (Fig. 5a), where they almost do not exist. In this extraction, samples at pH 4, 3.5 and 5, and to a lesser extent, pH 3 present concentrated REE. In the rest of the phases, concentrations diminish as solution acidity increases.

Clay minerals (Fig. 5b) show depleted REE but relatively concentrated in Solutions 6 and 7. In this phase, there is a positive correlation between LREE and pH. Organic matter and sulfuric minerals (Fig. 5e) also show depletion of REE contents, and more LREE than MREE and HREE. Analyzing Fe oxy-hydroxides phases (Fig. 5c and d), it is evident that the higher REE concentration occurs at the higher pH, reducing its concentration in the more acidic solution.

The behavior of REE in river water is far less constrained, due to the diversity of river chemistries and the complexity of solution-colloid interactions. Qualitatively at least, REE concentrations and fractionation in river waters are the result of pH-dependent reactions in the solution and at the interface with colloids. Analyzing La_{SN}/Lu_{SN} ratios from Table 2, again there are differences between samples with pH < 6 and more neutral samples. When comparing LREE and HREE a predominance of the heavier element is noted, evidenced by La_{SN}/Lu_{SN} < 1 in most acid samples, whereas in the 6th extraction and some extractions at pH 6 and 7, the relationship is inverted. The interpretation is that in a solution with acidic pH, LREE are preferred in the dissolved fraction, while HREE are associated with the particulate phase. This behavior is reversed at circumneutral pH, where LREE and MREE are preferentially adsorbed onto surfaces, while HRREs are preferentially dissolved in solution, or HREE are more easily released from sediment surfaces with increasing pH. Although REE concentrations from López-González et al. (2012) are not similar, REE behavior agrees. They observed a relative depletion in LREE as a consequence of the low pH values, which prevents the separation of LREE from solution to the suspended matter. Then, when acid neutralization occurs, an increase in the LREE content is related to the preferential separation of LREE compared to MREE and HREE.

Sediments generated as a consequence of mixing acid mine drainage with seawater present MREE enriched shape (evidenced by and La_{SN}/Gd_{SN} < 1) with three main fractionation patterns: the first displays the

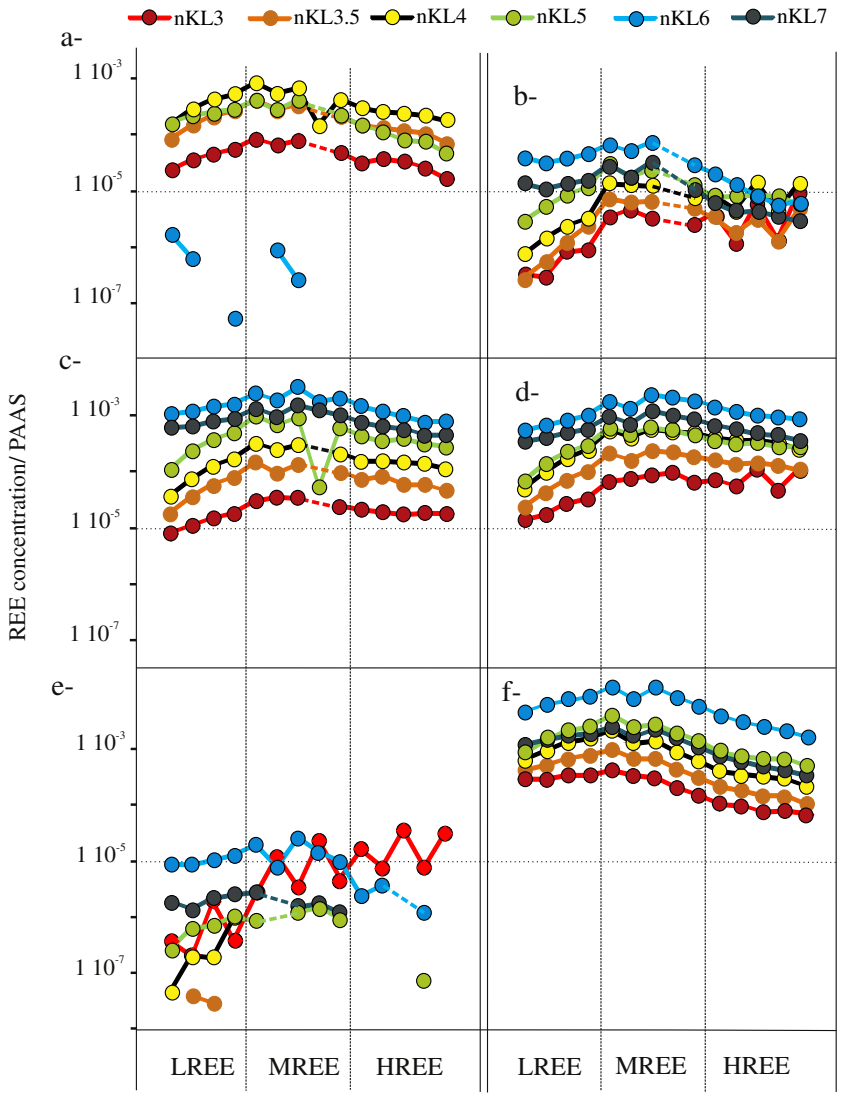

Fig. 5. The PASS-normalized REE distribution patterns for a) soluble salts (1° extraction), b) sorbed and exchangeable fraction in clay minerals (2° extraction), c) poorly ordered Fe^{3+} oxyhydroxides and oxyhydroxysulfates (3° extraction), d) highly ordered Fe^{3+} hydroxides and oxides (4° extraction), e) organic matter (5° extraction), and f) residual phase (6° extraction). 10^{-5} normalized concentration was added for comparison.

figure for soluble salts generated at pH < 6; the second shows a depletion in LREE over HREE evidenced in Fe oxy-hydroxides at pH < 6; whereas the third shows a relative increase in LREE over HREE in Fe oxy-hydroxides at pH > 6 and also in the residual phase. The evolution of these patterns reveals that pH is the key variable controlling REE fractionation in environments affected by acid mine drainage.

Salts are easily precipitated in any supersaturated solution. This could explain the high concentration REE associated with salts at lower pH, and also due to the amount of neoformed minerals, which are significantly greater at lower pH. This gives an idea of precipitation kinetics (opposite to pH), which could be the base for future studies. Another important detail worth mentioning is the REE behavior change at pH 6. Sediments generated at this pH present the highest REE concentrations, whereas when pH increases, REE concentrations decrease. These results encourage further research, where the PZC of specific minerals is calculated.

4. Conclusions

REE contents are retained in the newly minerals precipitated resulting from the interaction of AMD with seawater. REE increase their concentration in newly sediment generated at higher pH, reaching a maximum at pH 6 (i.e., > 1700 μg L^{-1}), whereas at around pH 7, REE are released again to solution.

Tinto River REE presents extremely high concentrations and low pH, exceeding 11,000 μg L^{-1}. When the pH begins to rise, they are quickly adsorbed, mainly onto soluble salts, but also onto Fe-oxi-hydroxides (prevailing crystalline ones). Later on, this is inverted; at pH 6, most REE are adsorbed onto Fe-oxi-hydroxides (in this case, mainly poorly ordered). Neither clay minerals nor organic matter are significant for REE adsorption at low pH.

REE PAAS-normalized patterns from the sediments along the Huelva Estuary (mixing between Tinto River AMD and seawater), showed an enrichment of the MREE and a relevant decrease in the REE contents in the downstream direction. Further, at acidic pH, LREE are preferentially in the dissolved fraction, while HREE are precipitated in the particulate phase. This behavior is reversed at circumneutral pH.

Leaching experiments performed on newly formed sediments demonstrate that the formation of low crystalline ochre precipitates and soluble salts (at pH < 5), should be the focus of further research, as they play a key role in controlling REE distribution and in the entire attenuation process.

Acknowledgments

The authors wish to thank the Spanish Ministry of Economy, Industry and Competitiveness for its financial support (SCYRE - CGL2016-78783-C2-1-R) and CONICET (Argentina) for KLL's external

fellowship. AMS has been funded through Programa de Fortalecimiento de las Capacidades I + D + I from Huelva University. The authors also wish to thank the thoughtful help of anonymous reviewers and Francois Galgani, the Chief Editor. Language assistance by native English speaker Wendy Walker is gratefully acknowledged.

References

Asta, M.P., MLl, Calleja, Pérez-López, R., Auqué, L.F., 2015. Major hydrogeochemical processes in an acid mine drainage affected estuary. Mar. Pollut. Bull. 91, 295–305.

Ayora, C., Macías, F., Torres, E., Nieto, J.M., 2015. Rare Earth Elements in Acid Mine Drainage. XXXV Reunión de la Sociedad Española de Mineralogía, Huelva. vol. S3–1. pp. S3–22.

Bigham, J.M., Schwertmann, U., Carlson, L., Murad, E., 1990. A poorly crystallized oxyhydroxysulfate of iron formed by bacterial oxidation of Fe(II) in acid mine waters. Geochim. Cosmochim. Acta 54, 2743–2758.

Borrego, J., López-González, N., Carro, B., 2004. Geochemical signature as paleoenvironmental markers in Holocene sediments of the Tinto River estuary (Southwestern Spain). Estuar. Coast. Shelf Sci. 61, 631–641.

Borrego, J., López-González, N., Carro, B., Lozano-Soria, O., 2005. Geochemistry of rare-earth elements in Holocene sediments of an acidic estuary: environmental markers (Tinto River Estuary, South-Western Spain). J. Geochem. Explor. 86, 119–129.

Borrego, J., Carro, B., Lopez-Gonzalez, N., de la Rosa, J., Grande, J.A., Gomez, T., de la Torre, M.L., 2012. Effect of acid mine drainage on dissolved rare earth elements geochemistry long a fluvial-estuarine system: the Tinto-Odiel Estuary (SW Spain). Hydrol. Res. 43, 262–274.

Braungardt, C.B., Achterberg, E.P., Elbaz-Poulichet, F., Morley, N.H., 2003. Metal geochemistry in a mine-polluted estuarine system in Spain. Appl. Geochem. 18, 1757–1771.

Brookins, D.G., 1989. Aqueous geochemistry of rare earth elements. In: Lippin, B.R., McKay, G.A. (Eds.), Reviews in Mineralogy. Geochemistry and Mineralogy of Rare Earth Elements. 21. pp. 201–223.

Caraballo, M.A., Rötting, T.S., Nieto, M., Ayora, C., 2009. Sequential extraction and DXRD applicability to poorly crystalline Fe- and Al-phase characterization from an acid mine water passive remediation system. Am. Mineral. 94, 1029–1038.

Carro, B., Borrego, J., López-González, N., 2007. Comportamiento del FE y otros metales en el agua de un sistema fluviomarino afectado por procesos de mezcla ácida (Ría de Huelva, España). Geogaceta 43.

Da Silva, E., Ferreira, E., Bobos, I., Matos, J., Patinha, C., Reis, A.P., Fonseca, E.C., 2009. Mineralogy and geochemistry of trace metals and REE in massive volcanic sulphide host rocks, stream sediments, stream waters and acid mine drainage from the Lousal mine area (Iberian Pyrite Belt, Portugal). Appl. Geochem. 24, 383–401.

De la Rosa, J.D., Chacón, H., Sánchez Campa, A.M., Carrasco, R., Nieto, J.M., 2001. Metodología y análisis de elementos traza-REE mediante ICP-MS del standard SARM1 (granito) y SARM4 (norita). Actas III Congreso Ibérico de Geoquímica. vol. 1. pp. 435–438 (ISBN: 84-930635-8-4).

Delgado, J., Pérez-López, R., Galván, L., Nieto, J.M., Boski, T., 2012. Enrichment of rare earth elements as environmental tracers of contamination by acid mine drainage in salt marshes: a new perspective. Mar. Pollut. Bull. 64 (1799–180).

Dold, B., 2003. Speciation of the most soluble phases in a sequential extraction procedure adapted for geochemical studies of copper sulfide mine waste. J. Geochem. Explor. 80, 55–68.

Elderfield, H., Upstill-Goddard, R., Sholkovitz, E.R., 1990. The rare earth elements in rivers, estuaries, and coastal seas and their significance to the composition of ocean waters. Geochim. Cosmochim. Acta 54, 971–991.

Fernandez-Caliani, J.C., Barba-Brioso, C., de la Rosa, J.D., 2009. Mobility and speciation of rare earth elements in acid minesoils and geochemical implications for river waters in the southern Iberian margin. Geoderma 149, 393–401.

Gagliano, W.B., Brill, M.R., Bigham, J.M., Jones, F.S., Traina, S.J., 2004. Chemistry and mineralogy of ochreous sediments in a constructed mine drainage wetland. Geochim. Cosmochim. Acta 68, 2119–2128.

Gaillardet, J., Viers, J., Dupré, B., 2014. Trace elements in river waters. In: Drever, J.I. (Ed.), Surface and Ground Water, Weathering, and Soils, Elsevier, Amsterdam. Treatise on Geochemistry, second edition. vol. 7 (7). pp. 195–235.

Gaillardet, J., Dupré, B., Allégre, C.J., Négrel, P., 1997. Chemical and physical denudation in the Amazon River basin. Chem. Geol. 142, 141–173.

Gammons, C.H., Wood, S.A., Nimick, D.A., 2005. Diel behavior of rare earth elements in a mountain stream with acidic to neutral pH. Geochim. Cosmochim. Acta 69 (15), 3747–3758.

García, M.G., Lecomte, K.L., Pasquini, A.I., Depetris, P.J., 2007. Sources of dissolved REE in mountainous streams draining granitic rocks, Sierras Pampeanas (Córdoba, Argentina). Geochim. Cosmochim. Acta 71, 5355–5368.

Gimeno Serrano, M.J., Auqué Sanz, L.F., Nordstrom, D.K., 2000. REE speciation in low-temperature acidic waters and the competitive effects of aluminum. Chem. Geol. 165, 167–180.

Hannigan, R.E., Sholkovitz, E.R., 2001. The development of middle rare earth element enrichments in freshwaters: weathering of phosphate minerals. Chem. Geol. 175, 495–508.

Lecomte, K.L., 2006. Control Geomorfológico en la Geoquímica de los ríos de Montaña, Sierras Pampeanas, Provincia de Córdoba, Argentina. (PHD Thesis) CIGeS. Facultad de Ciencias Exactas, Físicas y Naturales. Universidad Nacional de Córdoba, Argentina (312 pp.).

Lecomte, K.L., Milana, J.P., Formica, S.M., Depetris, P.J., 2008. Hydrochemical appraisal of ice- and rock-glacier meltwater in the hyperarid Agua Negra drainage basin, Andes of Argentina. Hydrol. Proc. 22 (13), 2180–2195.

Lecomte, K.L., Sarmiento, A.M., Borrego, J., Nieto, J.M., 2013. Metal Mobility Processes in an AMD-affected Estuary: Huelva Estuary, (SW Spain). V Regional Committee on Neogene Atlantic Stratigraphy – RCANS, Huelva, Spain.

Lecomte, K.L., Sarmiento, A.M., Borrego, J., Nieto, J.M., 2014. Movilidad de metales a partir de extracción secuencial: Estuario de Huelva (SO España) afectado por drenaje ácido de mina. Resumen extendido, III RAGSU. pp. 96–101 (ISBN: 978-987-544-598-7).

Lecomte, K.L., Maza, S.N., Collo, G., Sarmiento, A.M., Depetris, P.J., 2016a. Geochemical behavior of an acid drainage system: the case of the Amarillo River, Famatina (La Rioja, Argentina). Environ. Sci. Pollut. Res. 1–18. http://dx.doi.org/10.1007/s11356-016-7940-2.

Lecomte, K.L., Vieira da Silva-Filho, E., Bicalho, C.C., 2016b. Geochemical characterization in karst basin tributaries of The San Franciscan Depression: Corrente River, West Bahia, Brazil. J. S. Am. Earth Sci. 69, 119–130. http://dx.doi.org/10.1016/j.jsames.2016.03.011.

Leybourne, M.I., Goodfellow, W.D., Boyle, D.R., Hall, G.M., 2000. Appl. Geochem. 15, 695–723.

López-González, N., Borrego, J., Carro, B., Grande, J.A., de la Torre, M.L., Valente, T., 2012. Rare-earth element fractionation patterns in estuarine sediments as a consequence of acid mine drainage: a case study in SW Spain. Bol. Geol. Min. 123, 55–64.

McLennan, S.M., 1989. Rare earth elements and sedimentary rocks: influence of provenance and sedimentary processes. In: Lipin, B.R., McKay, G.A. (Eds.), Geochemistry and Mineralogy of Rare Earth Elements. Mineral. Soc. Am, Washington DC, pp. 169–196.

Medas, D., Cidu, R., De Giudici, G., Podda, F., 2013. Geochemistry of rare earth elements in water and solid materials at abandoned mines in SW Sardinia (Italy). J. Geochem. Explor. 133, 149–159.

Merten, D., Geletneky, J., Bergman, H., Haferburg, G., Kothe, E., Büchel, G., 2005. Rare earth patterns: a tool for understanding processes in remediation of acid mine drainage. Chem. Erde 65, 97–114.

Migaszewski, Z.M., Gałuszka, A., Dołęgowska, S., 2016. Rare earth and trace element signatures for assessing an impact of rock mining and processing on the environment: Wiśniówka case study, south-central Poland. Environ. Sci. Pollut. Res. 23, 24943–24959. http://dx.doi.org/10.1007/s11356-016-7713-y.

Morales, J.A., Borrego, J., San Miguel, E.G., López-González, N., Carro, B., 2008. Sedimentary record of recent tsunamis in the Huelva Estuary (southwestern Spain). Quat. Sci. Rev. 27, 734–746.

Nieto, J.M., Sarmiento, A.M., Canovas, C.R., Olias, M., Ayora, C., 2013. Acid mine drainage in the Iberian Pyrite Belt: 1. Hydrochemical characteristics and pollutant load of the Tinto and Odiel rivers. Environ. Sci. Pollut. Res. http://dx.doi.org/10.1007/s11356-013-1634-9.

Noack, C.W., Dzombak, D.A., Karamalidis, A.K., 2014. Rare earth element distributions and trends in natural waters with a focus on groundwater. Environ. Sci. Technol. 48, 4317–4326.

Nordstrom, D.K., 1982. The effect of sulfate on aluminum concentrations in natural waters: some stability relations in the system A12O3-SO3-H2O at 298 K. Geochim. Cosmochim. Acta 46, 681–692.

Nozaky, Y., Lerche, D., Sotto Alibo, D., Snidvongs, A., 2000. Geochim. Cosmochim. Acta 64, 3983–3994.

Olías, M., Cerón, J.C., Fernández, I., De la Rosa, J., 2005. Distribution of rare earth elements in an alluvial aquifer affected by acid mine drainage: the Guadiamar aquifer (SW Spain). Environ. Pollut. 135, 53–64.

Pagano, G., Guida, M., Tommasi, F., Oral, R., 2015. Health effects and toxicity mechanisms of rare earth elements - knowledge gaps and research prospects. Ecotoxicol. Environ. Saf. 115, 40–48. http://dx.doi.org/10.1016/j.ecoenv.2015.01.030.

Pasquini, A.I., Lecomte, K.L., Depetris, P.J., 2004. Geoquímica de ríos de montaña en las Sierras pampeanas: II. El río Los Reartes, Sierra de Comechingones, provincia de Córdoba, Argentina. Rev. Asoc. Geol. Argent. 59 (1), 129–140.

Pérez-López, R., Delgado, J., Nieto, J.M., Márquez-García, B., 2010. Rare earth element geochemistry of sulphide weathering in the São Domingos mine area (Iberian Pyrite Belt): a proxy for fluid–rock interaction and ancient mining pollution. Chem. Geol. 276, 29–40.

Protano, G., Riccobono, F., 2002. High contents of rare earth elements (REEs) in stream waters of a Cu–Pb–Zn mining area. Environ. Pollut. 117, 499–514.

Prudêncio, M.I., Dias, M.I., Waerenborgh, J.C., Ruiz, F., Trindade, M.J., Abad, M., Marques, R., Gouveia, M.A., 2011. Rare earth and other trace and major elemental distribution in a pedogenic calcrete profile (Slimene, NE Tunisia). Catena 87, 147–156.

Prudêncio, M.I., Valente, T., Marques, R., Sequeira Braga, M.A., Pamplona, J., 2015. Geochemistry of rare earth elements in a passive treatment system built for acid mine drainage remediation. Chemosphere 138, 691–700.

Querol, X., Alastuey, A., Lopez-Soler, A., Mantilla, E., Plana, F., 1996. Mineral composition of atmospheric particulates around a large coal-fired power station. Atmos. Environ. 30, 3557–3572.

Quispe, D., Pérez-López, R., Silva, L.F.O., Nieto, J.M., 2012. Changes in mobility of hazardous elements during coal combustion in Santa Catarina power plant (Brazil). Fuel 94, 495–503.

Rim, K.T., Koo, K.H., Park, J.S., 2013. Toxicological evaluations of rare earths and their health impacts to workers: a literature review. Saf. Health Work 4, 12–26.

Rosado, D., Usero, J., Morillo, J., 2016. Ability of 3 extraction methods (BCR, Tessier and protease K) to estimate bioavailable metals in sediments from Huelva estuary (Southwestern Spain). Mar. Pollut. Bull. 102, 65–71.

Sahoo, P.K., Tripathy, S., Equeeniddin, S.M., Panigrahi, M.K., 2012. Geochemical characteristics of coal mine discharge vis-à-vis behaviour of rare earth elements at Jaintia

Hills coalfield, northeastern India. J. Geochem. Explor. 112, 235–246.
Sarmiento, A.M., DelValls, A., Nieto, J.M., Salamanca, M.J., Caraballo, M.A., 2011. Toxicity and potential risk assessment of a river polluted by acid mine drainage in the Iberian Pyrite Belt (SW Spain). Sci. Total Environ. 409, 4763–4771.
Sarmiento, A.M., Lecomte, K.L., Borrego, J., Nieto, J.M., 2015. Efecto del pH en la Movilidad de Metales en un Estuario Afectado por Drenajes Ácidos de Mina. 20. Maclapp. 139–140.
Sarmiento, A.M., Olías, M., Nieto, J.M., Cánovas, C.R., Delgado, J., 2009. Natural attenuation processes in two water reservoirs receiving acid mine drainage. Sci. Total Environ. 407, 2051–2062.
Sharifi, R., Moore, F., Keshavarzi, B., 2013. Geochemical behavior and speciation modeling of rare earth elements in aciddrainages at Sarcheshmeh porphyry copper deposit, Kerman Province, Iran. Chem. Erde 73, 509–517.
Sholkovitz, E.R., 1995. The aquatic chemistry of rare earth elements in rivers and estuaries. Aquat. Geochem. 1, 1–34.
Tyler, G., Carrasco, R., Nieto, J.M., Pérez-López, R., Ruiz, M.J., Sarmiento, A.M., 2004. In: Optimization of major and trace element determination in acid mine drainage samples by ultrasonic nebulizer-ICP-OES (USN-ICP-OES). Pittcon Conference (Chicago, USA). (pp. 9000–1000).
Van Geen, A., Boyle, E.A., Moore, W.S., 1991. Trace metal enrichments in waters of the Gulf of Cadiz, Spain. Geochim. Cosmochim. Acta 55, 2173–2191.
Welch, S.A., Christy, A.G., Isaacson, L., Kirste, D., 2009. Mineralogical control of rare earth elements in acid sulfate soils. Geochim. Cosmochim. Acta 73, 44–64.
Zhao, F., Cong, Z., Sun, H., Ren, D., 2007. The geochemistry of rare earth elements (REE) in acid mine drainage from the Sitai coal mine, Shanxi Province, North China. Int. J. Coal Geol. 70, 184–192.